UNCONVENTIONAL RESOURCES TECHNOLOGY CONFERENCE
FUELED BY SPE • AAPG • SEG

URTeC: 3722883

Lithologically-Controlled Variations of the Least Principal Stress with Depth and Resultant *Frac Fingerprints* During Multi-Stage Hydraulic Fracturing

Mark Zoback*[1], Troy Ruths[2], Mark McClure[3], Ankush Singh[3], Arjun Kohli[1], Brendon Hall[2], Rohan Irvin[3], and Malcolm Kintzing[4], 1. Stanford University, 2. Petro.ai, 3. ResFrac, 4. Henry Resources

Abstract

We present observational data and modeling results which support the hypothesis that the degree of vertical to horizontal hydraulic fracture propagation during multi-stage hydraulic fracturing is largely controlled by variations of the least principal stress with depth. It is obvious that monotonic variations of the least principal stress with depth imply either upward or downward hydraulic fracture growth. More interestingly, we present several case studies in which direct measurements show layer-to-layer stress variations of the least principal stress as large as ~10 MPa (~1500 psi) which are lithologically controlled. Using two different types of analysis approaches, we investigate complex patterns of vertical and horizontal hydraulic fracture growth from the Midland Basin. In each case, we show that pattern of hydraulic fracture propagation (and resultant drainage volumes) are largely governed by the detailed variation of the magnitude of the least horizontal stress with depth and exact position of a given stage. In gun barrel view, this complex pattern we refer to as a *frac fingerprint* for convenience. The frac fingerprint depends on the exact vertical position of a frac stage with respect to the variations of the least principal stress in the layers both above and below the stage depth. We show how frac fingerprints can vary along the length of a well because of the way its trajectory encounters lithofacies along its length. We briefly discuss the implication of these concepts for choosing optimal well spacings and landing depths and the relationships between hydraulic fracture geometry and drainage volumes.

Introduction

It was established 65 years ago that hydraulic fractures should propagate perpendicular to the minimum horizontal principal stress, S_{hmin} (Hubbert and Willis, 1957). While there have been abundant observations consistent with this concept, recent experiments in the Eagleford Formation (Raterman et al., 2017) and the Permian Basin at HFTS-1 and HFTS-2 (Gale et al., 2018: 2021) have added appreciable new data confirming this concept. Hubbert and Willis (1957) also argued that the magnitude of the least

principal stress governs the pressure required for propagation of hydraulic fractures. In most areas, of interest to development of unconventional oil and gas reservoirs, the least principal stress is the least principal horizontal stress, S_{hmin} (see recent review by Lund Snee and Zoback (2022) of stress orientations and magnitudes in unconventional sedimentary basins in North America). Thus, knowledge of S_{hmin} and its variations with depth is especially important in unconventional oil and gas reservoirs exploited with multi-stage hydraulic fracturing in horizontal wells. Of specific interest in this paper is the variation of S_{hmin} with depth. The least principal stress governs the degree to which hydraulic fractures propagate vertically, either upward or downward, depending on S_{hmin} magnitudes above, within and below the horizontal section of well commonly referred to as the lateral. Significant vertical propagation can limit successful exploitation of the targeted formation and defines the number of laterals required to exploit productive zones at multiple depth intervals or stacked pay. Hence, optimizing the depths and number of laterals needed to exploit stacked pay as well as the optimal well spacing at different depths will be closely related to how the magnitude of S_{hmin} varies with depth.

Fortunately, abundant information about stress orientation and relative magnitude is available in many regions of interest. Fig. 1 shows a map of the direction and relative magnitudes of the horizontal principal stresses in the Permian Basin from Lund Snee and Zoback (2022) as well as relative stress magnitudes. Note the locations of HFTS-1 in the Midland Basin (characterized by normal and strike-slip faulting) and the location of HFTS-2 in the Delaware Basin (a normal faulting area) which are discussed later in the paper. Note that uniform stress orientations characterize the Midland Basin (S_{Hmax} is approximately E-W throughout) while a significant, but coherent, rotation of the S_{Hmax} direction is seen from north to south in the Delaware Basin. The great majority of these stress indicators come from numerous, consistently oriented drilling-induced tensile fractures and stress induced wellbore breakouts in vertical wells (see review in Zoback, 2007) meaning that there are no significant variations of stress orientation (and thus, the direction of hydraulic fracture propagation) over the depth ranges of interest in this study.

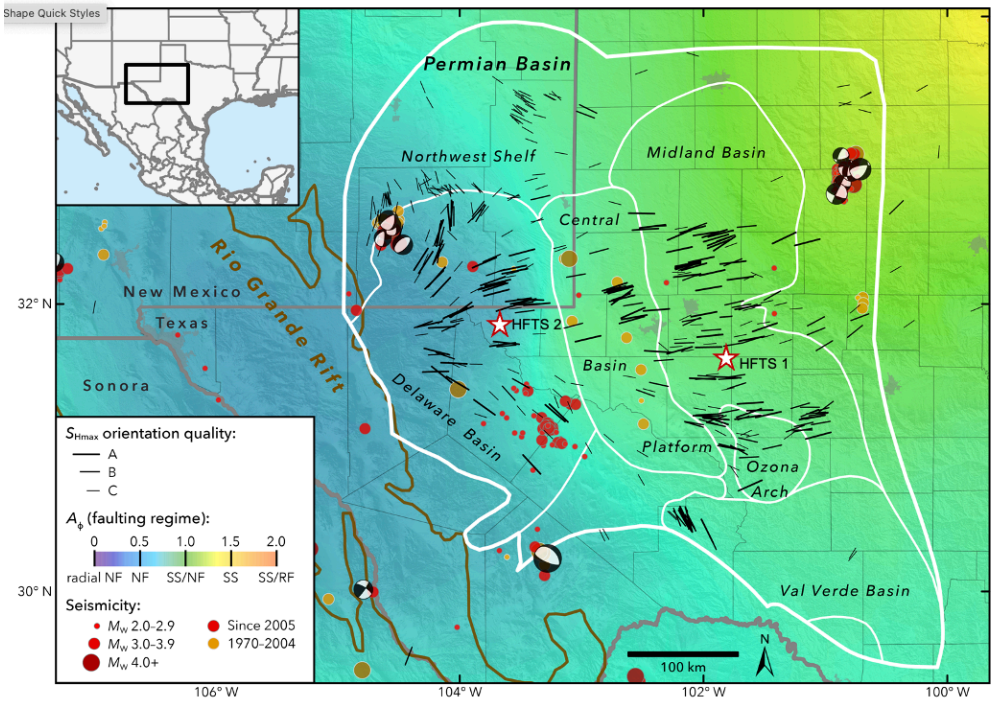

Figure 1. *State of stress in the Permian Basin, west Texas and southeast New Mexico (from Lund Snee and Zoback (2022). Directions of S_{Hmax} are shown as well as relative stress magnitudes expressed in terms of the parameter Aϕ.*

While the orientation of S_{Hmax} and S_{hmin} do not change over the depth range of interest (see discussion in Lund Snee and Zoback, 2022), of principal interest in this paper are pronounced variations of the magnitude of S_{hmin} with depth. Fig. 2 (from Kohli and Zoback, 2021) shows variations of the magnitude of S_{hmin} from eleven DFITs in various wells ranging from the Sprayberry and Dean formations at relatively shallow depth down through the lower part of the Middle Wolfcamp formation. In this figure, all measurement depths have been shifted slightly to the same stratigraphic position based on the logs in the vertical well 7SU pilot. As can be seen, measured values of the least principal stress fluctuate by as much as 10-15 MPa (1500-2175 psi). As discussed below, the variation of the least principal stress shown in the figure do not reflect random scatter or faulty measurements. They correlate with lithologic changes – the higher values of the least principal stress are associated with lithofacies with higher clay plus TOC. Kohli and Zoback (2021) point out that the low values of S_{hmin} are consistent with the predictions from frictional faulting theory for a normal faulting area (the gray shaded bar), an observation supported by the rapid onset of microseismic events as soon as pumping starts during stages in the more brittle lithofacies.

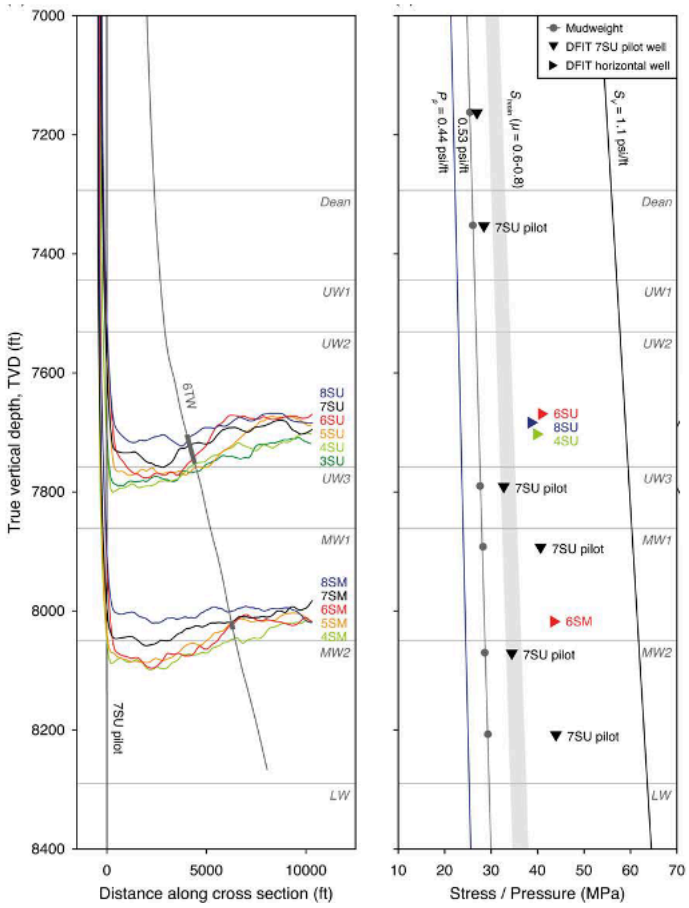

Figure 2. Well trajectories and lithofacies of HFTS-1 wells are shown on the left. The right shows DFIT measurements in various wells slightly shifted to be at the appropriate stratigraphic depth using the vertical pilot well 7SU pilot as reference. Hydrostatic pore pressure, the mud gradient, the lower bound of S_{hmin} predicted from frictional faulting theory and the overburden stress are shown for reference.

Similarly, Fig. 3 (modified from Singh and Zoback, 2022) shows a suite of DFIT stress measurements from a proprietary study of 18 wells drilled from 3 pads in a 3x3 mile area. Again, we observe considerable variations in the values of S_{hmin} with depth. The orange line represents the frictional limit analogous to the gray bar in Fig. 2. In the Upper Wolfcamp, values of S_{hmin} vary by about 1300 psi over a relatively small range of depths. In the Middle Wolfcamp there is less scatter, but still about 1000 psi variations over relatively small depth ranges. As for the data shown in Fig. 2, we will show that these variations of stress magnitude result from changes in lithology

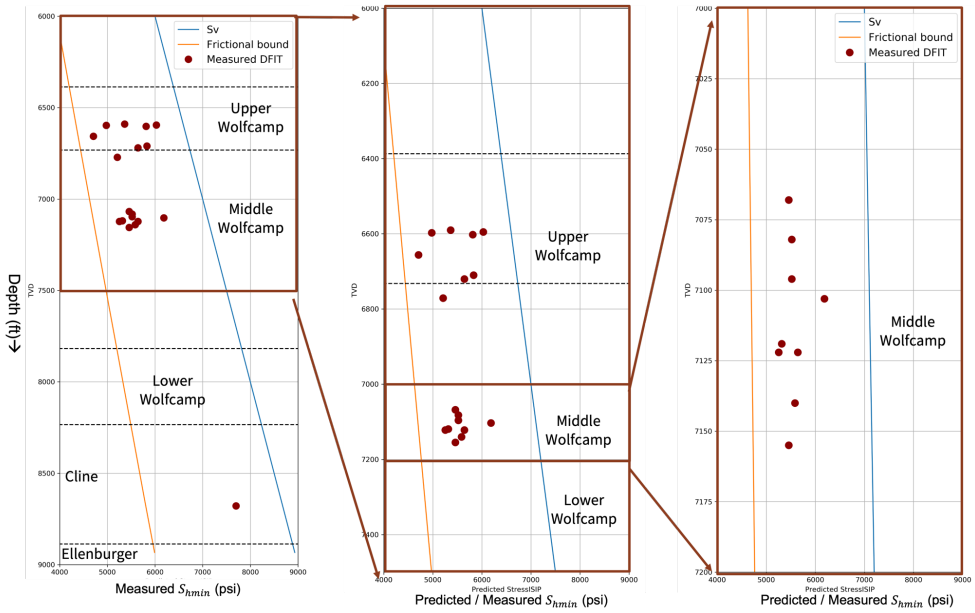

Figure 3. A proprietary compilation of S_{hmin} measurements in the Wolfcamp and Cline formations obtained from DFIT measurements in 18 wells in close proximity located in the Midland Basin (modified from Singh and Zoback, 2022).

While the cases considered in detail below come from unconventional wells principally targeting the Wolfcamp sequence in the Permian Basin, Xu et al. (2019) present a series of S_{hmin} measurements with depth in the Utica/Pt. Pleasant sequence in Ohio with variations on the order of 1000 psi. The profound effect these variations have on hydraulic fracture propagation was addressed by Singh et al. (2020). Ma and Zoback (2017, 2020) present profiles of S_{hmin} values along the length of horizontal wells in the Woodford formation in Oklahoma in which the well trajectories cross-three distinct lithofacies and least principal stress values vary by as much as 2000 psi. No hydraulic fracturing was attempted in the stages with the highest values of the least principal stress. These stages correspond to lithofacies with the most clay + TOC, where the magnitude of the least principal stress was approximately that of the overburden. Alalli and Zoback (2018) present similar results in horizontal wells in the Marcellus that encounter multiple lithofacies and values of the least principal stress that vary markedly. In the stages in which the least principal stress was approximately that of the overburden, microseismic data indicate that horizontal hydraulic fractures were formed. Zoback and Kohli (2019) show the extreme variations of the least principal stress over very limited depth ranges that were obtained by numerous mini-frac tests in three vertical wells at the multi-well site in western Colorado in the 1980's. While S_{hmin} values in sands increase with depth and pore pressure as expected in a normal faulting area, the least principal stress was measured to be essentially the same as the overburden stress in shales and mudstones.

Theory and/or Methods

In this section we describe three methodologies that are fundamental to understanding frac fingerprints and the way in which the exact depth of a specific frac stage, in relation to layer-to-layer variations of the least principal stress, S_{hmin}, result in different patterns of horizontal and vertical hydraulic fracture propagation and proppant distribution. We term these patterns frac fingerprints because in gun-barrel view, they reflect a unique pattern reflecting stress magnitudes within, above and below a given stage. We first present a brief overview of viscoplastic stress relaxation (VSR) theory that makes it possible to quantitatively predict a continuous profile of the magnitude as a function of depth. The theory posits that layer-to-layer stress magnitude variations principally depend on lithology. Second, we present the theoretical basis for simulating hydraulic fracture propagation and proppant distribution for individual frac stages. Finally, we present a geomechanically-based, machine-learning methodology that computes

drainage volumes around horizontal wells as informed by stress variations with depth (as predicted by VSR) but ultimately constrained by matching production data from pre-existing wells in an area.

As geophysical well logs provide continuous profiles of lithologic and petrophysical information, constructing a profile of stress magnitudes with depth derived from well log data would be highly desirable. A number of studies have attempted to create models which use sonic logs to predict variations of S_{hmin} with depth, either using a uniaxial strain model (e.g., Eaton, 1969; Anderson et al., 1973) or modifications of the uniaxial strain model that adds tectonic, thermal and poroelastic terms (*e.g.*, Thiercelin and Plumb, 1994; Blanton and Olson, 1999) as typically required to fit one or two measured values of S_{hmin}. These methods, which we will refer to as the *Extended Eaton* method, are limited by the assumptions that the rock is purely elastic and that stress magnitudes that exist today result from instantaneous application of both the overburden and tectonic stresses (or strains) - a highly questionable geologic assumption. Several recent studies in which multiple direct measurements of S_{hmin} as a function of depth were available have demonstrated the failure of this approach to match measured values. This has been shown in the Wolfcamp formation of the Midland Basin at the site where the data shown in Fig. 3 were obtained (Singh and Zoback, 2022), the Utica/Pt. Pleasant formations in Ohio (Xu, 2020) and the Niobrara formation in Colorado (McCormack et al., 2021).

Previous studies related the concept of viscoelastic stress relaxation (VSR) to lithology-dependent variations of the magnitude of S_{hmin} with depth in unconventional oil and gas plays in a semi-quantitative manner. Studies have reported results for the Barnett shale (Sone and Zoback, 2014b), the Woodford formation in Oklahoma (Ma and Zoback, 2020 and the Niobrara formation in Colorado (McCormack et al., 2021). As shown in Figs. 4a,b,c (from Zoback and Kohli, 2019 derived from data in Sone and Zoback, 2012) laboratory experiments using samples from three unconventional shale formations show that the amount of viscoplastic creep in a given period of time depends on the mass volume of highly compliant constituents such as clay and organic matter. Figs. 4 d,e illustrate that viscoplastic creep under constant stress conditions (similar to the way in which the laboratory measurements were carried out is equivalent to stress relaxation under constant strain conditions (such as would be expected in stable continental interiors. A simple way to think about VSR and stress magnitudes is that the more a rock tends to deform as a function of time (viscous deformation), the lower the *differences* between the three principal stresses become. In normal and strike-slip faulting areas (which characterize nearly all unconventional plays), as the differences in principal stresses decrease, S_{hmin} would increase, thus becoming closer in magnitude to the overburden stress, S_V.

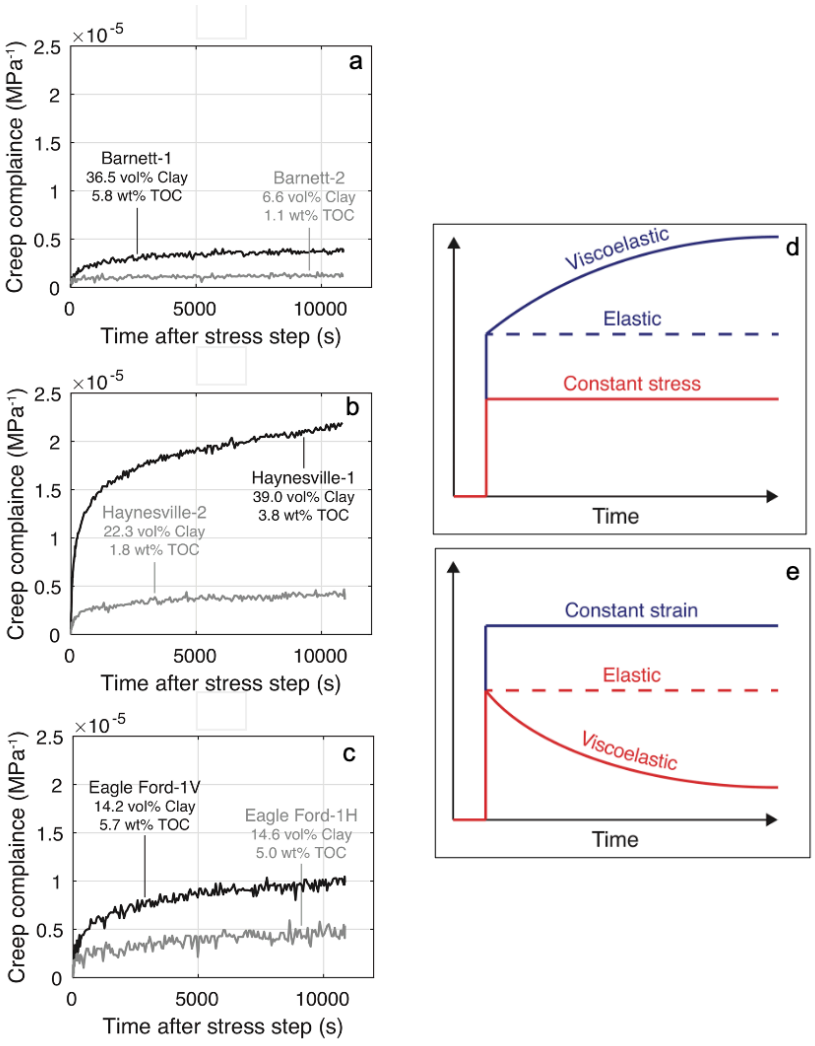

Figure 4. *Creep strain normalized by differential stress (creep compliance) as a function of time after Sone and Zoback (2014). (a) Barnett clay-rich and -poor end members. (b) Haynesville. (c) Eagle Ford-1 vertical and horizontal. (c) Schematic of laboratory experimental technique in which creep strain as a function of time is measured at constant stress but is equivalent to stress relaxation as a function of time at constant strain as shown in (d). From Zoback and Kohli (2019)*

In two case studies presented below, the VSR concept was applied quantitatively following Singh and Zoback (2022) to produce a continuous profile of S_{hmin} magnitudes with depth by utilizing a statistical model to parameterize a viscoelastic stress relaxation constitutive with commonly available geophysical logs in nearby vertical wells. Because a key element of the VSR concept is that changes in amount of clay plus TOC in various lithofacies are responsible for layer-to-layer stress variations, the slight shifting of the measurements to a common stratigraphic depth was an important first step in this type of analysis. Fig. 5 (from Singh and Zoback, 2022) shows how remarkably well the quantitative application of VSR fits the stress measurements presented in Fig. 3 at all scales. The center and right panels of Fig. 5 are especially revealing as it shows that the relatively rapid fluctuations of S_{hmin} with depth are predictable based on lithologic variations using VSR theory. Thus, what might be mistakenly interpreted as scatter in the stress measurements in the Upper and Middle Wolfcamp in the left panel, are actually variations of the magnitude of S_{hmin} caused by variations of lithology.

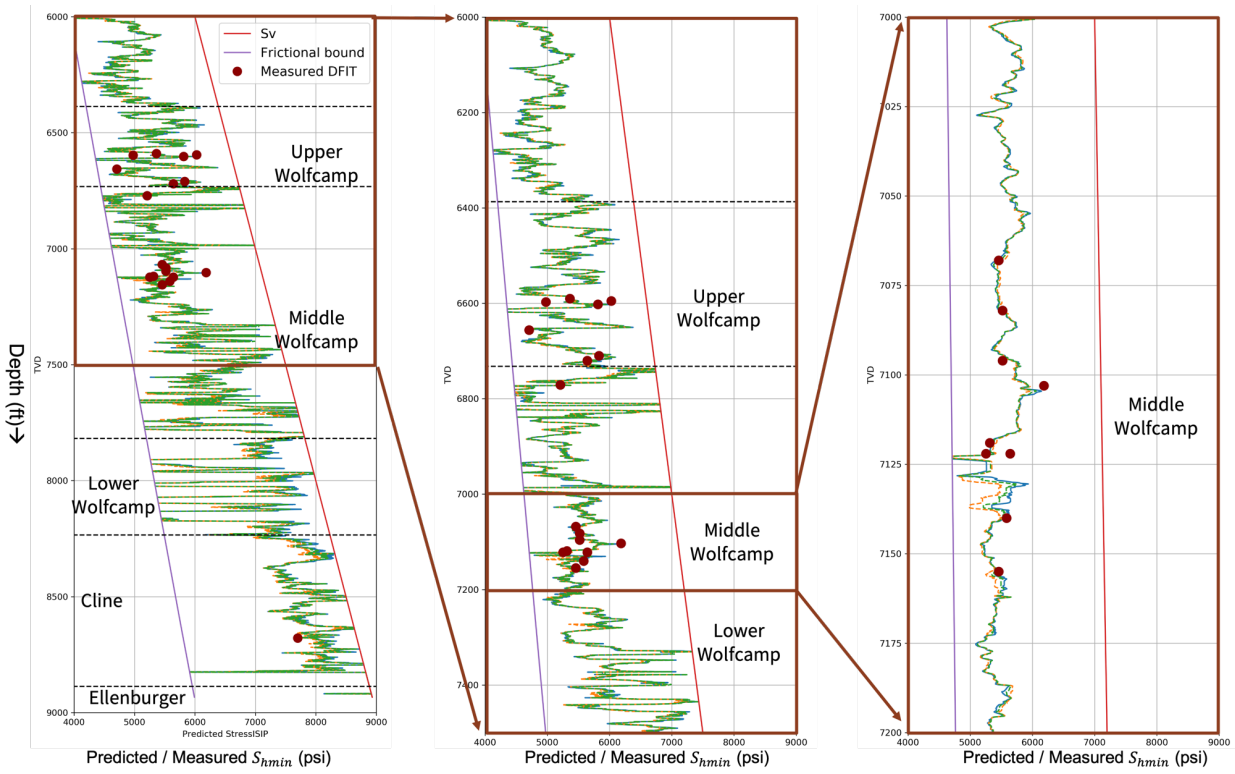

Figure 5. Theoretically predicted values of the least principal stress data shown in Fig. 3 using the VSR technique described in detail by Singh and Zoback (2022) match the measured values shown in Fig. 3.

A less rigorous prediction of stress magnitudes utilizing the VSR concept with the HFTS-1 data is shown in Fig. 6 (from Kohli and Zoback, 2021). In this case, the log of clay + TOC provides the opportunity to estimate variations of stress magnitude with depth between the depths where direct measurements are available. As mentioned above, the relatively brittle rocks (very low clay + TOC) are consistent with the prediction of frictional faulting theory using the overburden stress and pore pressure at the appropriate depth. These are the relatively low stress measurements. The Wolfcamp lithofacies associated with the relatively high stress values in UW2, MW1 and MW2 are each associated with relatively high clay + TOC values of approximately 30%. Thus, the stress profile shown in the right panel of Fig. 6 honors 1) the available DFITS (and ISIPs from various frac stages, Fig. A1 in Kohli and Zoback) as indicated by the solid line, 2) stress magnitudes in lithofacies with high clay + TOC as indicated by the dashed line and 3) frictional equilibrium in low clay + TOC intervals (dashed lines where no DFITS are available).

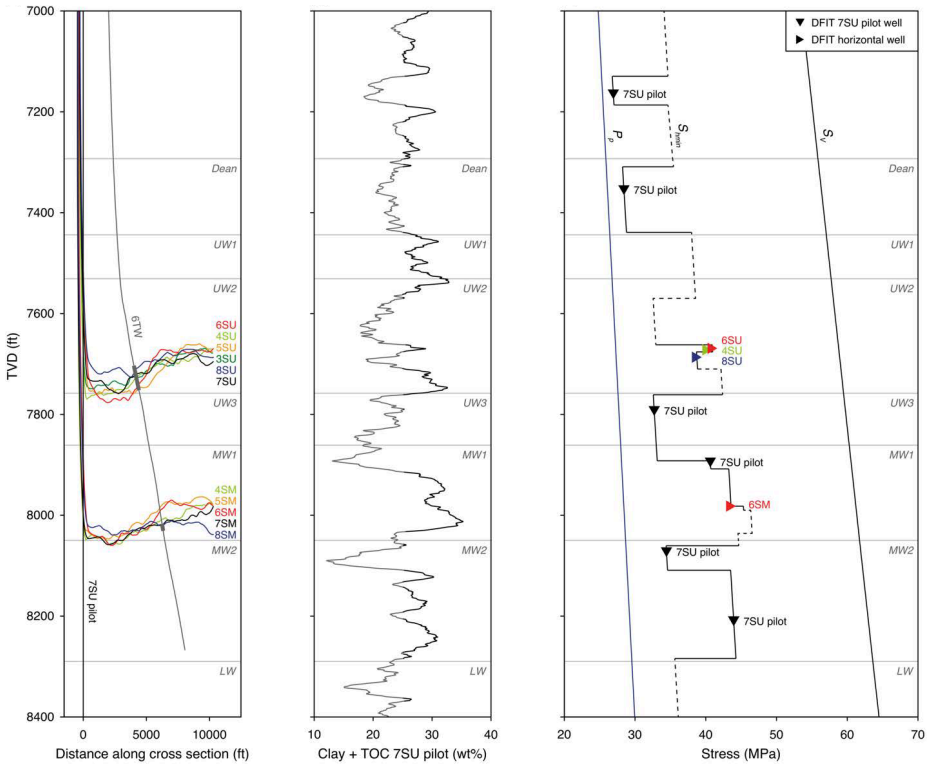

Figure 6. Well trajectories and lithofacies of HFTS-1 wells are shown in the left panel, the variation of clay + TOC (wt %) are shown in the middle panel as determined from well logs in well 7SU pilot and a continuous profile of the magnitude of the least principal stress, S_{hmin}, is shown on the right, honoring the measured values shown, ISIP from individual frac stages (not shown) and inferences about stress magnitude from clay + TOC content (from Kohli and Zoback, 2021).

The simulations of hydraulic fracture propagation shown below were performed with a combined hydraulic fracturing, wellbore, and reservoir simulator (McClure et al., 2022). In the simulator, hydraulic fractures are represented discretely with planar elements; the well(s) are represented with linear elements; and the matrix is represented by volumetric elements – either a rectilinear or corner point grid. The matrix mesh is non-conforming to the fracture elements; a sub-meshing technique is used to achieve numerical accuracy, even if the matrix mesh is coarse relative to the radius of investigation. In each timestep, the simulator enforces a set of balance equations: mass balance on fluid components, proppant types, and water solutes; energy balance; and (in the wellbore) momentum balance. In addition, the simulator solves the equations of linear elastic continuum mechanics to calculate the stress changes caused by fracture opening and by pressure and temperature changes in the matrix. All equations are solved simultaneously in every element in every timestep. Fracture propagation is based on linear elastic fracture mechanics, using the MuLTipEl algorithm developed by Dontsov et al. (2022). Stress interaction between fracture elements is calculated using the displacement discontinuity method from Shou et al. (1997).

We further develop the frac fingerprint concept by characterizing basin-level productivity trends and pad optimization (well spacing, landing target, and completion design) using a geomechanics-informed machine learning workflow. Productivity drivers are encoded as features to train a supervised machine learning model (XGBoost, Chen and Guestrin 2016) that predicts 12-month cumulative oil production, validated using a hold-one-out cross-validation strategy. As shown in Fig 7 for a case study in the Midland Basin, a vertical profile of the magnitude of the least principal stress was developed using the VSR methodology following Singh and Zoback (2022) using quality-controlled median ISIP values from wells in a study area for calibration. The predicted S_{hmin} profile is shown in the first panel as well as the ISIPs used to calibrate the stress model. Based on the stress profile and other available data (such as microseismic locations, well-to-well communication, spacing degradation, etc.) we calculated unique frac

fingerprints that represent principal drainage volume surrounding hypothetical stages at three depths where direct stress measurements were available. For the purpose of these example calculations, no surrounding wells were included in the analysis resulting in symmetric drainage volumes around each stage. As can be seen in the second panel, the drainage volume for a stage at the depth shown in the WCA principally produces from the upper part of the WCA due to upward propagation of hydraulic fractures into a lower stress zone not shown in the figure. A hydraulic fracture from a stage located at the depth shown in the thin lithofacies WCB1 propagates upward into the lower part of the WCA thus producing from that interval. A stage located near the middle of the WCB3 propagates upward into the lower stress zone in the WCB2 and produces from that formation. Individual well production data are aggregated into pad groups that were completed and brought online within 180 days of each other. The right panel of Fig. 7 shows that the production model trained using frac fingerprints as illustrated predicts 12-month actual production data from 196 pads in the area with 89% cross-validation accuracy.

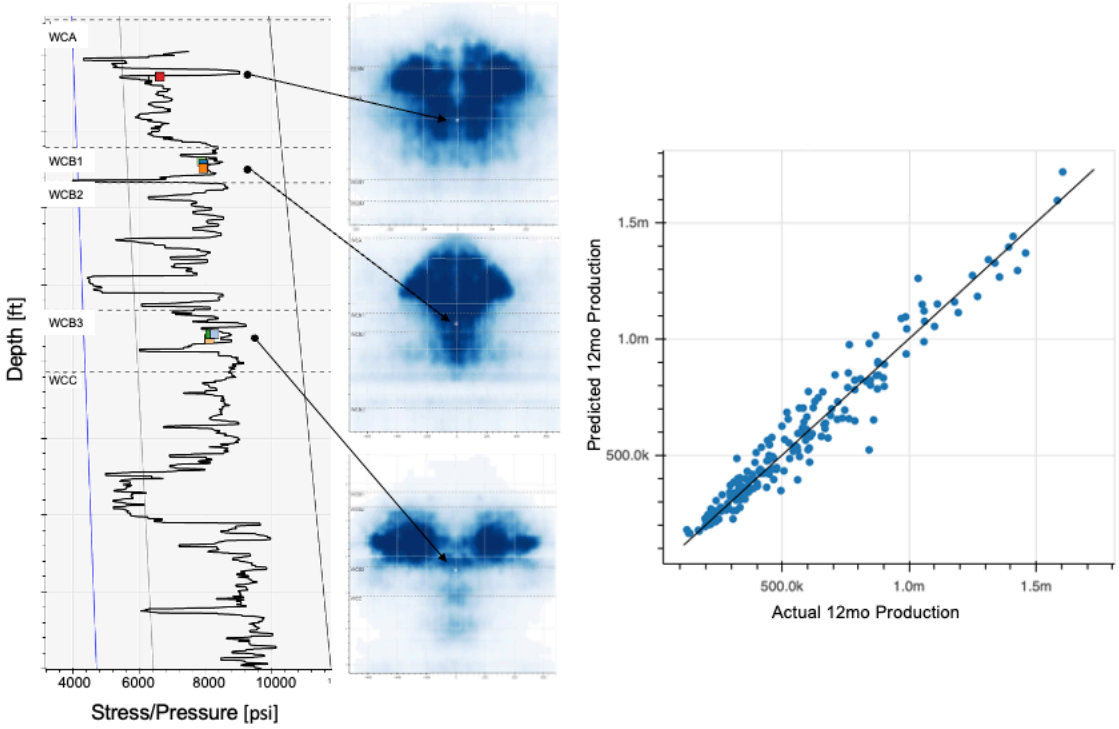

Figure 7. The workflow associated with the geomechanically-constrained production model is illustrated using an example from the Midland Basin. On the left is the variation of the magnitude of the least principal stress (with the overburden stress, pore pressure and least principal stress assuming frictional equilibrium for reference) as well as the median ISIPs used to calibrate the model in the manner described by Singh and Zoback (2022). The machine learning production model produced the frac fingerprints shown in the second panel, defined as the apparent drainage area surrounding the stage. The panel on the right shows that the drainage model developed for the region (in addition to other completion and reservoir factors) predicts the actual 12-month well production with 89% accuracy.

Results

The first three implementations of the technologies described utilize hydraulic fracture modeling with the simulator to visualize frac fingerprints. In each case, we simulate a single stage using the best available knowledge of the completion and stimulation and petrophysical parameters. The fourth implementation utilizes the methodology illustrated in Fig. 7 to evaluate the concept of frac fingerprints in the context of the drainage area around wells applied to the development of wells drilled in stacked pay in the Midland Basin.

The first hydraulic fracture modeling case we consider is HFTS-1 At this site, viscoplastic stress relaxation varies with lithology, as seen in the stress profile shown in Fig. 6 (Kohli and Zoback, 2021). A

full description of this experiment is provided by Ciezobka et al. (2018). In brief, eleven horizontal wells were drilled and over 400 hydraulic fracturing stages were carried out in the Upper and Middle Wolfcamp formations. About 600 feet of core was acquired from a slant core through the hydraulically fractured volume between the horizontal wells. As seen in Figs. 2 and 6, an unusual aspect of the HTFS-1 well trajectories is that they were all drilled with a step-like configuration such that the stages near the toe are approximately at the same stratigraphic depth about 100 feet higher than stages near the heel. The result is that hydraulic fracturing stages near the heel and toe are in different places in the stress layering. As a consequence, they have different frac fingerprints. The stress model in Fig. 6 is shown by the colors on the left side of Fig. 8. The right side of Fig. 8 shows the results of hydraulic fracture modeling at three specific depths along well 6SM where color shows hydraulic fracture aperture and the white star shows the true vertical depth of the stage. Figs. 8a,b represent fracture modeling for two actual stages in the well corresponding to the white stars on the left side of the figure. Fig. 8a represents a stage in a high stress layer near the toe of the well in the middle of layer MW1 in Fig. 6 and Fig. 8b represents a stage near the heel of the well that on the boundary between a high stress layer MW1 and the low stress layer MW2. Fig. 8c represents a hypothetical stage just a few tens of feet below the heel stage shown in Fig. 8b near the top of layer MW2. Note that the toe stage in the relatively high stress layer (Fig.8a) has a fingerprint that indicates that most of the propped hydraulic fracture is mostly in the formation in the upper part of MW2, below the depth of the stage. The heel stage at the boundary between the high and low stress layers indicates relatively little horizontal hydraulic fracture propagation at the depth of the stage but considerable propagation downward into the lower stress MW2 (similar to the toe stage) but also upward propagation into layer UW3. Fig. 8c, the hypothetical stage in the low stress lithofacies near the top of MW2 shows, as might be intuitively expected, lateral hydraulic fracture propagation that is well constrained by the higher stresses above and below the hypothetical landing depth.

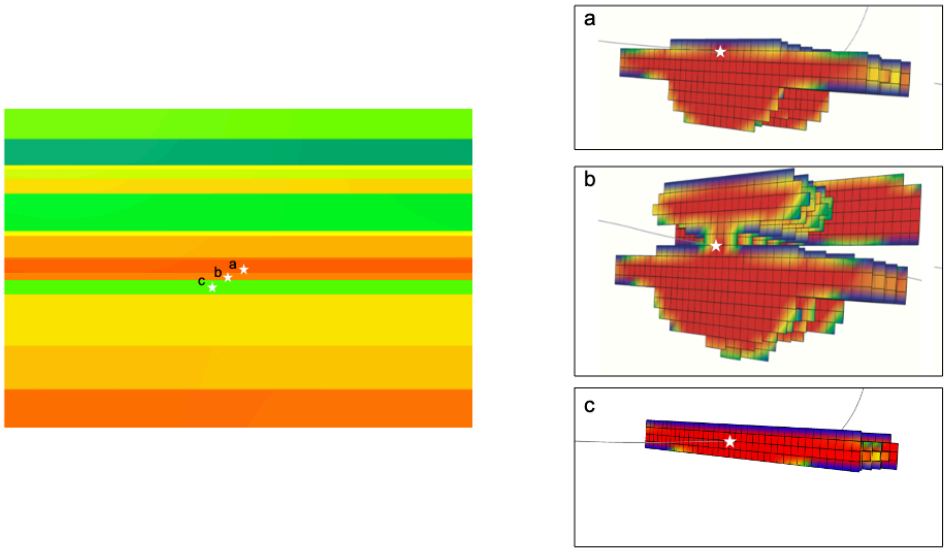

Figure 8. The stress model shown in Fig. 6 is shown on the left using a color scale, warmer colors representing higher values of the S_{hmin}. As described in the text the white stars labeled a and b on the left correspond to the depths of stages near the toe (a) and heel (b) of well 6SM. The star labeled c is at a hypothetical depth in the low stress layer just below the depth of the heel of the well. Panels a, b and c on the right show the modeled frac fingerprints in terms of hydraulic fracture aperture for stages at the three respective depths shown on the left. Dark blue indicates essentially no aperture after fracture closure.

While there is no independent evidence that supports the details of three frac fingerprints shown, available microseismic data are generally consistent with the vertical propagation predicted by these models (see discussion in Kohli and Zoback, 2021). Additionally, it is obvious that there are a number of factors that influence hydraulic fracture propagation. The modeling effort shown in Fig. 8 is intended to highlight the importance of the precise depth of a stage in the context of variations of the magnitude of S_{hmin} with depth,

keeping completion parameters and rock properties held constant. It is thus obvious that there are profound implications for the corresponding drainage volumes (are the hydraulic fractures producing from the desired formations?) and well spacing.

An overview of the operational and scientific studies associated with the HFTS-2 experiments was presented by Zhao et al. (2021). The project was carried out in the Delaware Basin (see Fig. 1) and focused on various units of the Wolfcamp formation. In addition to a thoroughly logged and instrumented vertical pilot well, a slant cored well and a number of new child wells were drilled in the vicinity of several pre-existing parent wells. Of most interest in this paper are the hydraulic fracture modeling efforts undertaken to optimize well spacing and completion design at the and Pudugramam et al. (2022). The HFTS-2 hydraulic fracture models shown in Fig. 9 (from Pudugramam et al., 2022) represent one stage that was part of a larger modeling effort calibrated with key observations from field data, which included: horizontal and vertical well DAS/DTS/DSS fiber recordings, downhole microseismic arrays, pressure gauges, core-through data, image logs, DFITs, proppant-in-cuttings analysis, interference tests and almost 2 years of oil, gas and water production data.

The stress profile on the left side of Fig 9 utilized available well logs and DFIT tests to compute a vertical profile of the magnitude of the least principal stress based on the VSR model following the methodology of Singh and Zoback (2022) illustrated in Fig. 5. Over the lower half of the stress model, values of the least principal stress represented by green to orange color indicates approximately 3000 psi. The predicted extent of hydraulic fracture propagation is shown on the right for representative stages of two actual wells shown at the positions indicated on the left. The propped fracture aperture is shown by the color with green indicating areas where fracture propagation occurred but without proppant. The severe upward propagation of the hydraulic fractures is intuitively predictable from the lower stress magnitudes shown above the depth of the wells. As discussed by Pudugramam et al. (2022), this upward propagation was confirmed by fiber data in the nearby vertical well. While this aspect of hydraulic fracture propagation is quite similar for the two wells, frac fingerprint*s* based on propped fracture areas for the two cases is quite different. For example, half lengths for the two wells are quite different and there is modest downward growth of hydraulic fractures associated with well b.

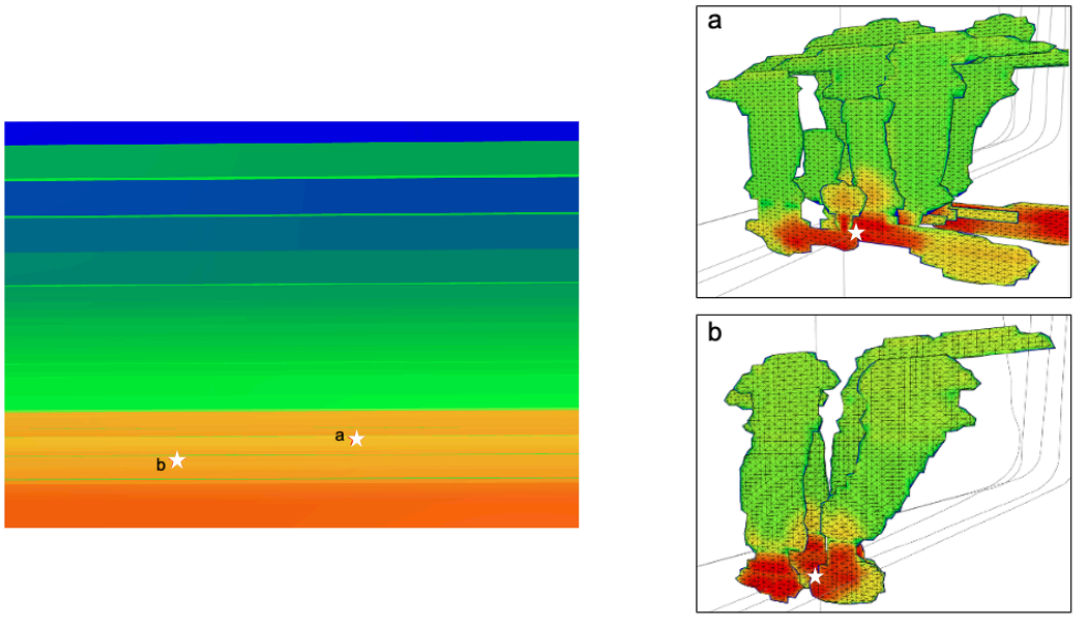

Figure 9. A stress model developed for HFTS-2 using the VSR technique illustrated in Fig.5 is shown on the left with warmer colors representing higher values of the S_{hmin}. The white stars labeled a and b correspond to the depths of stages in two different wells targeting different lithofacies. The panels on the right show modeled frac fingerprints in terms of hydraulic fracture aperture for the depths shown on the left. The markedly upward propagation of the hydraulic fractures has been confirmed by fiber data in a nearby vertical well (from Pudugramam et al., 2022).

We also modeled hydraulic fracture propagation for two hypothetical Wolfcamp wells at the site where the proprietary data shown in Fig. 3 was obtained and for which the continuous stress model shown in Fig. 5 was developed. The hydraulic fracture models shown in Fig. 10 correspond to a hypothetical stage in a low stress layer at a depth of 6672 ft, close to measured data point in the Upper Wolfcamp and a stage at 6740 ft, close to two measured points near the Upper/Middle Wolfcamp boundary (as indicated in the center panel of Fig. 5). Unfortunately, no completion data was available for these wells. The hydraulic fracture models were developed using nominal parameters: a 100 ft. stage length, 4, equally spaced perforation clusters and injection at 50 bbl/min for 2 hours. In this case the hydraulic fractures show only moderate vertical growth, a concentration of proppant in the near wellbore area and very long fracture half lengths, most of which are predicted to have no aperture after fracture closure. This said, a closer look reveals that propagation from the deeper landing zone (b) is mostly upward due to the lower stresses in the overlaying layers. However, propagation from the well in the low stress landing zone (a) is not as well contained as was seen in Fig. 8c because the low stress is too thin. Rather, propagation is predicted to occur both above and below the well, resulting in considerable overlap of the propped areas from the two wells. While this example is hypothetical, the depths chosen for analysis correspond to the depths of measured stress via DFITs at the toe of actual wells. Thus, if these two wells were in close proximity, they would have been competing for resources in the same formations.

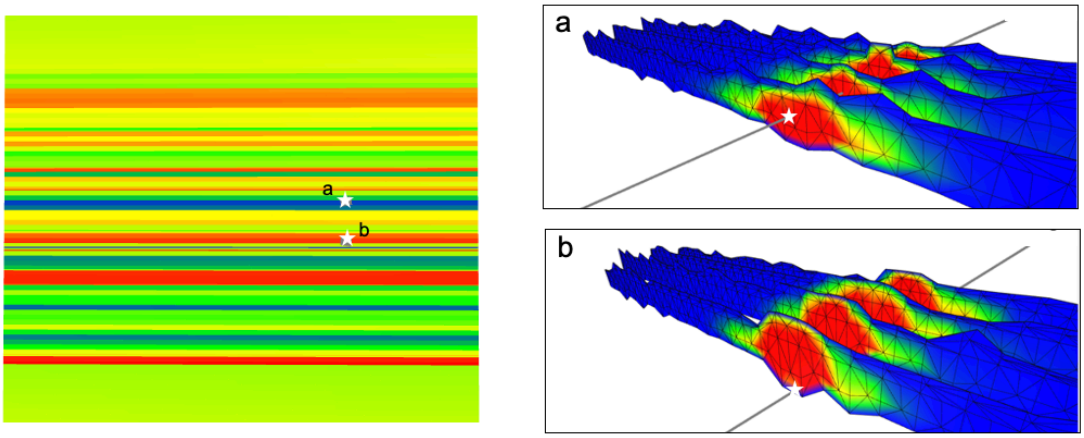

Figure 10. The stress model shown in Fig.5 has been used to constrain two hypothetical hydraulic fractures in a low stress zone (a) and high stress zone (b) as described in the text.

Finally, we apply the frac fingerprint concept using the data-driven methodology from Fig. 7 to an actual five well development in the Midland Basin. In this case study, the productivity model was trained on modern offset wells in the county and, in a blind test, predicted with 94% accuracy cumulative 12 month oil volumes for the five well pad. We compare the drainage as inferred by frac fingerprints to geochemical signatures of cuttings and fluids that identify the formations contributing to production (pad X in Ge et al., 2022). As shown in Fig. 11, the landing targets of the pad are in the upper part of the Wolfcamp B lithofacies (a), the mid-point of the Wolfcamp B (b), and the Wolfcamp B Lower lithofacies (c). The combined frac fingerprints for the pad show considerable vertical drainage overlap, suggesting the stacking configuration of a and c is sub-optimal. Mostly downward propagation is predicted from the upper two wells whereas some downward, but mostly upward propagation is predicted from the lower two wells. The vertical distribution of production inferred by the geochemical analysis is superimposed on the frac fingerprints in the figure. As shown, these two independent estimates of drainage largely agree. The geochemical data shows production from the three targeted intervals with minor production from the WFMP A or WFMP C. The differences when viewed on a well-to-well basis most likely results from shared production between nearby wells due to their close spacing and the stacking in this development configuration.

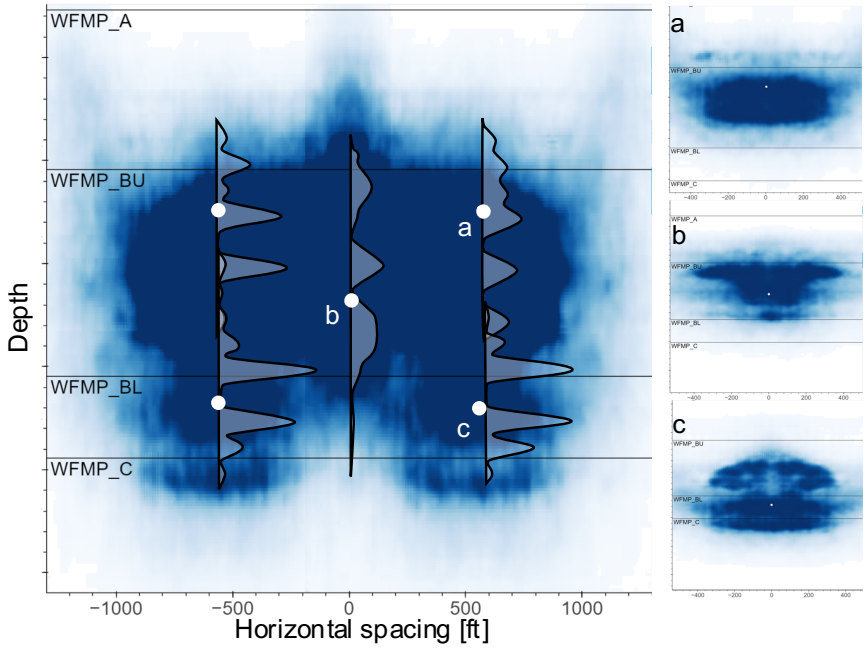

Figure 11. The predicted drainage zones of five Wolfcamp wells in the Midland Basin using the frac fingerprint workflow illustrated in Fig. 7. Individual frac fingerprints (a-c) aggregate to estimate pad drainage. This analysis reveals considerable overlap of the vertical drainage suggesting that stacking these targets is not an optimal development configuration. In addition, little production is predicted from the WFMP A and the WFMP C. As explained in the text, the aggregate production from the pad is consistent with cumulative production profiles determined from independent geochemical signatures (Ge et al., 2022).

Discussion

The frac fingerprint concept leads directly to new exploitation strategies of unconventional reservoirs that should improve both recovery factors and well economics through optimized pad designs. Recovery factors from unconventional reservoirs have remained extremely low despite 15 years of concerted effort, hundreds of thousands of horizontal wells and millions of individual frac stages. We argue here that variations of the magnitude of the least principal stress with depth needs to be taken into account for determining optimal landing zones and well spacing. The critical importance of documenting (through measurement and modelling) lithology-dependent, layer-to-layer variations of the least principal stress is clearly seen in the models shown in Figs. 8-11. For example, the modeling of the HFTS-1 data set suggests that not only is there the expected vertical propagation from high stress layers to low stress layers (the case shown in Fig. 8a), lateral propagation may not be occurring at the depth of the landing zone (the case shown in Fig. 8b) and that even semi-quantitative approximations of the presence of stress-related frac barriers can be useful in understanding hydraulic containment (the case shown in Fig. 8c). Modelling of the HFTS-2 data set shown in Fig. 9, explains the well-documented vertical and horizontal extent of hydraulic fracture propagation, but demonstrates that much of the hydraulic fracture area does not contribute significantly to production (as the hydraulic fracture aperture is essentially zero after the hydraulic fracture closes) and the propped half-lengths of hydraulic fractures generated at different stratigraphic levels is markedly different. Thus, when exploiting stacked pay, optimal well spacing would likely be different for wells drilled at different depths. In the study shown in Fig. 10 related to modeling hydraulic fracture propagation for two wells associated with the stress model shown in Fig. 5, the overall geometry of the hydraulic fractures was not unusual. However, the implication that wells drilled through different pay zones might be producing from the same formation illustrates the importance of modeling efforts (based on a reliable profile of S_{hmin} magnitude with depth) prior to determining optimal landing zones or well spacing.

As mentioned above, the hydraulic fracture modeling in the case of HFTS-2 (Fig. 9) was particularly well-constrained by comprehensive monitoring, including fiber in both a nearby vertical well and offset horizontal wells. These observations were critical in confirming the vertical and lateral extent of hydraulic fracture propagation shown in the figure. More importantly, the 'best case' simulation from the optimization algorithm had a 60% increase in NPV/section over the base case design (Pudugramam et al., 2022). Even with high-quality diagnostics, modeling hydraulic fracture propagation is inexact, due the inherent simplifying assumptions associated with numerical modeling. Moreover, the models involve a number of formation parameters, some of which are poorly constrained. One example is the parameter fracture toughness, the required energy near the tip of a propagating hydraulic fracture needed to overcome the strength of the rock. There is difficulty knowing how toughness varies with lithology, how to scale laboratory measurements of fracture toughness to the field. There is uncertainty about how much fracture toughness might increase as hydraulic fractures grow larger and whether fracture toughness is anisotropic, making hydraulic fracture propagation more difficult vertically than horizontally. In the cases of Figs. 8 and 10, a reasonable value of ~3000 psi-in$^{1/2}$ was used, and fracture toughness was assumed to increase with the square root of hydraulic fracture length (Shlyapobersky, 1985; Economides and Nolte, 1985). No toughness anisotropy was assumed. In the case shown in Fig. 9, horizontal and vertical toughness was varied to match the fracture arrival times indicated by the fiber data and vertical toughness was assumed to be 25% larger than horizontal toughness. Regardless of such uncertainties, the three cases shown in Figs. 8-10 show how dependent hydraulic fracture propagation at each site can be, as result of the depth of a stage with respect to the varying magnitude of the least principal stress with depth. Based on analysis of 62 DFIT tests, McClure et al. (2022) concluded that net pressures are mostly in the range of 100-250 psi, but could be as much as 500 psi in some cases. As net pressure not only includes the effect of fracture toughness on fracture propagation but pumping rate- and viscosity-dependent friction in the wellbore and perforations, it is clear that the magnitude of the variations of the magnitude of S_{hmin} documented above are quite large and thus have a significant effect on hydraulic fracture propagation.

The geomechanically-constrained productivity modeling approach discussed in Figs. 7 and 11 uses machine learning to automatically fit importance factors to unknowns using well production data. Because data from an ensemble of wells is used, it aggregates geologic and completion parameters over a given area and appreciable volume of rock. Further work will be required to know (in each unconventional play) how large a geographic area will be applicable to a specific pad. Using a large population of wells for training builds confidence that the model is generalizing productivity trends from a variety of pad designs and is less sensitive to specific formation parameters. We can use this approach to evaluate development scenarios within the bounds of the training data set. As shown in Fig. 12, the frac fingerprints of the five well pattern discussed in Fig. 11 (shown on the left) involved significant overlap of drainage areas. Through an optimization process we determined that nearly equivalent 12 month oil production could be achieved with four wells with the configuration shown on the right, which includes small but important adjustments to targeting and spacing. Economics for the four well were considerably better than the five well pad, and resulted in improved containment in the WFMP B, and better protected the wells from production decline degradation commonly associated with tight well spacing.

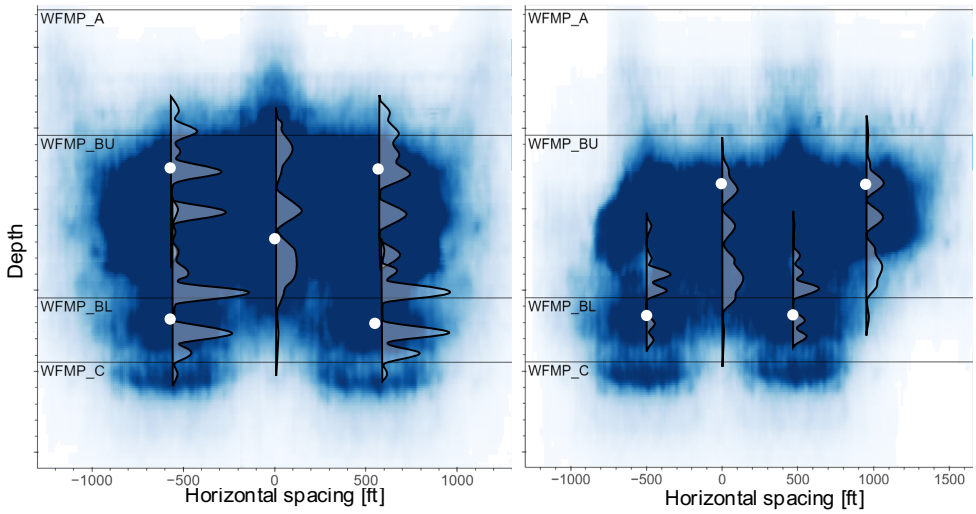

Figure 12. Using a geomechanically-constrained production model, it was determined that the production associated with a 5 well pattern of wells drilled in the Midland Basin could have been achieved by four wells in the positions shown on the right.

.

Conclusions

A number of case studies were discussed that show significant variations of the magnitude of the least principal stress with depth from various unconventional oil and gas producing areas. We show that even in the same formation, lithofacies characterized by different amounts of clay + TOC can significantly affect stress magnitudes in a manner that can be quantitatively predicted, or estimated, in the context of viscoplastic stress relaxation.

We presented five case studies in the Wolfcamp series of formations of the Permian Basin. In each case, stacked pay is being exploited by wells at multiple landing depths. Both types of analysis we presented illustrated the importance of the exact depth of a stage in the context of variations of the magnitude of the least principal stress with depth. Minor changes of the depth of a stage can significantly affect the detailed combination of vertical and horizontal hydraulic fracture propagation and proppant placement that controls the drainage area around a well. We have termed this the *frac fingerprint* for convenience.

Hence, determination of optimal well spacing and landing depths, which is likely not the same for different landing zones, whether through modeling or field testing needs to be done in a context of a well constrained profile of the magnitude of the least principal stress with depth.

References

Alalli, A.A. and M.D. Zoback. 2018. Microseismic evidence for horizontal hydraulic fractures in the Marcellus Shale, southeastern West Virginia, The Leading Edge, https://doi.org/10.1190/tle37050356.1.

Anderson, R. A., D. S. Ingram and A. M. Zanier. 1973. Determining fracture pressure gradients from well logs: Journal of Petroleum Technology, 25, 1259–1268, doi: 10.2118/4135-PA.

Chen, Tianqi, and C. Guestrin. 2016. Xgboost: A scalable tree boosting system. In Proceedings of the 22nd ACM SIGKDD International Conference on Knowledge Discovery and Data Mining, San Francisco, CA, USA, 13-17 August. https://dl.acm.org/doi/10.1145/2939672.2939785

Blanton, T. L., and J. E. Olson. 1999. Stress magnitudes from logs: Effects of tectonic strains and temperature: SPE Reservoir Evaluation & Engineering, 2, 62–68, doi: 10.2118/54653-PA.

Ciezobka, Jordan, J. Courtier, and J. Wicker. 2018. Hydraulic fracturing test site (HFTS) – Project overview and summary of results. Paper URTeC: 2937168 Presented at the Unconventional Resources Technology Conference held in Houston, Texas, USA, 23-25 July 2018.

Dontsov, Egor, C. Hewson, and M. McClure. 2022. A new crack propagation algorithm that enables accurate simulation of propagation across thin layers in a practical field-scale fracturing model. Paper SPE 209146-MS presented at the SPE Hydraulic Fracturing Technology Conference, The Woodlands, TX.

Eaton, B. A., 1969, Fracture gradient prediction and its application in oilfield operations: Journal of Petroleum Technology, 21, 1353–1360, doi: .2118/2163-PA.

Economides, M. and K. Nolte, eds.. 1989, Reservoir Stimulation, 3rd Edition, Wiley ISBN-13: 978-0471491927

Gale, J. F.W., S.J. Elliott and S.E. Laubach. 2018. Hydraulic fractures in core from stimulated reservoirs: core fracture description of HFTS slant core, Midland Basin,West Texas. https://doi.org/10.15530/urtec-2018–2902624

Kohli, A. and M.D. Zoback. 2021. Stratigraphically controlled stress variations at the Hydraulic Fracture Test Site-1 in the Midland Basin, TX. Energies. 14 (24) https://doi.org/10.3390/en14248328

Gale, J.F.W., S.J. Elliot, B.G. Rysak, C.L. Ginn, N. Zhang R.D. Meyers, and S.E. Laubach. 2021. Fracture Description of the HFTS-2 Slant Core, Delaware Basin, West Texas. Presented at the Unconventional Resources Technology Conference, Houston, Texas, 26–28 July. URTEC-2021-5175-MS. https://doi.org/10.15530/urtec-2021-5175.

Lund Snee, J.-E. and M.D. Zoback. 2021. State of stress in areas of active unconventional oil and gas development in North America. Am. Assoc. Pet. Geol. Bull. 106, n. 2, 355-385.

Ma, X. and M.D. Zoback. 2017. Lithology-controlled stress variations and pad-scale faults: A case study of hydraulic fracturing in the Woodford Shale, Oklahoma. Geophysics, 82 (6) https://doi.org/10.1190/GEO2017-0044.1

Ma, X. and M.D. Zoback. 2020. Predicting lithology-controlled stress variations in the Woodford shale from well log data via viscoplastic relaxation. SPE Jour., 25, 2534–2546, doi:10.2118/201232-PA.

McClure, M., G. Fowler and M. Picone. 2022. Best practices in DFIT interpretation: comparative analysis of 62 DFITS from nine different shale plays. SPE-205297-MS, Paper presented at the SPE International Hydraulic Fracturing Technology Conference & Exhibition, Muscat, Oman, 11 - 13 January 2022.

McClure, Mark, C. Kang, S. Medam, C. Hewson, and E. Dontsov. 2022 ResFrac Technical Writeup. Available online: https://arxiv.org/abs/1804.02092.

McCormack, K., M. D. Zoback and W. Kuang. 2021. A case study of vertical hydraulic fracture growth, stress variations with depth and shear stimulation in the Niobrara shale and Codell sand, DJ Basin, Colorado. Interpretation, Vol. 9, No. 4 (November 2021); p. SG59–SG69.

Pudugramam, Sriram, R. Irvin, M. McClure, G. Fowler, F. Bessa, Y. Zhao, J. Han, L. Han, A. Kohli, M. D. Zoback, A. A. Savitski and G. Ugueto. 2022. Optimizing well spacing and completion design using simulation models calibrated to the Hydraulic Fracture Test Site 2 (HFTS-2) dataset. Paper URTeC: 3723620. This paper was prepared for presentation at the Unconventional Resources Technology Conference held in Houston, Texas, USA, 20-22 June 2022.

Raterman, K. T., H.D. Farrell, O.S. Mora, A.L. Janssen, G.A. Gomez, S. Busetti, J. McEwen, M. Davidson, K. Friehauf, J. Rutherford, R.Reid, G. Jin, B. Roy and M. Warren. 2017. Sampling a Stimulated Rock Volume: An Eagle Ford Example (pp. 24–26). https://doi.org/10.15530/urtec-20172670034

Shlyapobersky, J., 1985. Energy analysis of hydraulic fracturing, 26th U.S. Symposium on Rock Mechanics, Rapid City, South Dakota, 26-28, 1985.

Shou, K.-J., E. Siebrits and S. L. Crouch. 1997. A higher order displacement discontinuity method for three-dimensional elastostatic problems. International Journal of Rock Mechanics and Mining Sciences 34 (2): 317-322, doi: 10.1016/S0148-9062(96)00052-6.

Singh, A., M.D. Zoback and M. McClure. 2020. Optimization of multi-stage hydraulic fracturing in unconventional reservoirs in the context of stress variations with depth. Paper SPE-201739-MS. In Proceedings of the SPE Annual Technical Conference and Exhibition.

Singh, A., and M.D. Zoback. 2022. Predicting variations of the least principal stress with depth: Application to unconventional oil and gas reservoirs using a log-based viscoelastic stress relaxation model. Geophysics, Vol. 87, No. 3 (May-June 2022); p. 1–12. https://doi.org/10.1190/geo2021-0429.1.

Sone, H. and M.D. Zoback. 2014. Time-dependent deformation of shale gas reservoir rocks and its long-term effect on the in situ state of stress. Int. J. Rock Mech. Min. Sci. **2014**, 69, 120–132, doi:10.1016/j.ijrmms.2014.04.002.

Sone, H. and M.D. Zoback. 2014. Time Viscous relaxation model for predicting least principal stress magnitudes in sedimentary rocks. J. Pet. Sci. Eng., 124, 416–431, doi:10.1016/j.petrol.2014.09.022.

Thiercelin, M. J., and R. A. Plumb, 1994, A core-based prediction of lithologic stress contrasts in east Texas formations: SPE Formation Evaluation, 9, 251–258, doi: 10.2118/21847-PA.

Xu, S., F.S. Rassouli, F.S. and M.D. Zoback. 2017. Utilizing a viscoplastic stress relaxation model to study vertical hydraulic fracture propagation in the Permian Basin. In Proceedings of the SPE/AAPG/SEG Unconventional Resources Technology Conference. https://doi.org/10.15530/urtec-2017–2669793

Zhao, Y., F. Bessa, V. Sahni, S. Pudugramam and S. Liu. 2021. Key Learnings from Hydraulic Fracturing Test Site-2 (HFTS-2), Delaware Basin. Presented at the Unconventional Resources Technology Conference, Houston, Texas, 26–28 July. URTEC-2021-5229-MS. https://doi.org/10.15530/urtec-2021-5229.

Zoback, M. D. 2007. Reservoir Geomechanics. Cambridge University Press. ISBN-10: 9780521146197

Zoback, M.D. and A.H. Kohli. 2019. Unconventional Reservoir Geomechanics; Cambridge University Press. ISBN 9781107087071.